Journal of
Materials Chemistry B

REVIEW

Check for updates

Cite this: J. Mater. Chem. B, 2019, 7, 1581

Semicrystalline physical hydrogels with shape-memory and self-healing properties

Oguz Okay

Received 20th October 2018,
Accepted 19th November 2018

DOI: 10.1039/c8tb02767f

rsc.li/materials-b

Synthetic hydrogels are generally amorphous in nature without any order at the molecular level. This is in contrast to biological gels containing ordered aggregates contributing significantly to their mechanical performance. Semicrystalline hydrogels, first developed in 1994, are moderately water-swollen hydrogels containing crystalline domains. Recent work shows that physically cross-linked semicrystalline hydrogels belong to one of the groups of mechanically strong and highly stretchable hydrogels exhibiting melt-processability, self-healing and shape-memory functions. They can undergo an abrupt and reversible change from a solid-like to a liquid-like state at the melting temperature, opening up several applications such as shape-memory hydrogels, injectable gels, chemical motors, and smart inks for 3D or 4D printing. In this review article, recent advances in the field of semicrystalline physical hydrogels prepared from hydrophilic and hydrophobic vinyl monomers *via* a free-radical mechanism are summarized. Synthesis–molecular structure–property relations of semicrystalline hydrogels, current challenges and future directions are also discussed.

1. Introduction

Hydrogels are intelligent, soft and wet materials with great similarity to biological systems and therefore they attract significant attention for various applications, including in tissue and biomedical engineering, artificial organs, sensors, and actuators.[1–6] Although hydrogels are generally considered as fragile, significant progress has been achieved in the past two decades in the synthesis of mechanically strong and tough hydrogels by creating energy dissipation mechanisms in the gel network.[7–9] Recent achievements in terms of the mechanical parameters of "second generation" hydrogels such as Young's modulus E, tensile strength σ_f, and the fracture energy G reveal that they are not any more fragile than the classical ones (Fig. 1).[10–17] They are mechanically strong and tough materials with a high modulus (~100 MPa), tensile strength (~10 MPa), and fracture energy (~20 kJ m^{-2}), thus approaching the mechanical properties of many biological systems.

Hydrogels are generally amorphous in nature without any order at the molecular level. This is in contrast to biological gels containing ordered aggregates, mainly in their cross-link domains, contributing significantly to their mechanical performance and smart functions.[19,20] The first attempt to create crystalline order in chemically cross-linked hydrogels was made by Osada and co-workers in 1994.[21–26] Semicrystalline hydrogels were synthesized by a simple solution terpolymerization of acrylic acid, *n*-octadecyl acrylate, and the chemical cross-linker *N*,*N*-methylene(bis)acrylamide in ethanol in the presence of a radical initiator. After replacing the solvent ethanol with water, moderately water-swollen hydrogels containing alkyl crystals were obtained. After the pioneering work of Osada's group, several research groups prepared chemically cross-linked semicrystalline hydrogels *via* free-radical copolymerization of hydrophilic and hydrophobic monomers and investigated the effects of the synthesis conditions on their microstructures and

Istanbul Technical University, Department of Chemistry, 34469 Maslak, Istanbul, Turkey. E-mail: okayo@itu.edu.tr

Oguz Okay

Oguz Okay received his PhD degree in polymer chemistry from Vienna Technical University, Austria in 1981. He worked in the TÜBİTAK Marmara Research Center, University of Stuttgart, Technical University of Clausthal, Helmholtz Zentrum Berlin, Eastern Mediterranean University, and Kocaeli University. Currently, he is a full Professor of physical chemistry at Istanbul Technical University and a principal member of The Turkish Academy of Sciences (TUBA). He is the recipient of several awards including the Georg-Forster Research Award from Germany (2015), TUBITAK Science Award (2005), and Turkish Chemical Society Honorary Member Award (2006). His research expertise includes design of soft and smart polymeric materials. He has authored 170+ peer-reviewed papers cited ~9000 times.

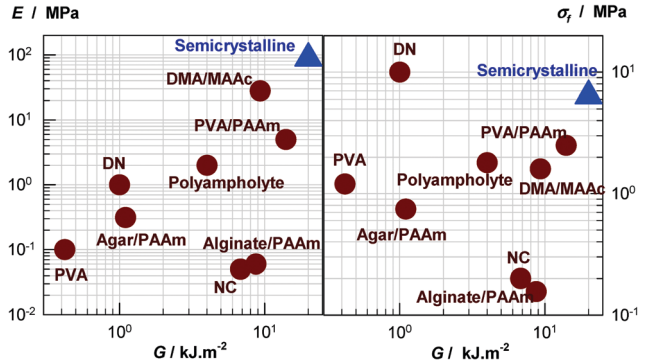

Fig. 1 The mechanical parameters, the modulus E, tensile strength σ_f, and fracture energy G of second generation hydrogels.[10–17] The abbreviations are explained in ref. 18. Reprinted with permission from ref. 34. Copyright 2016 Elsevier Ltd.

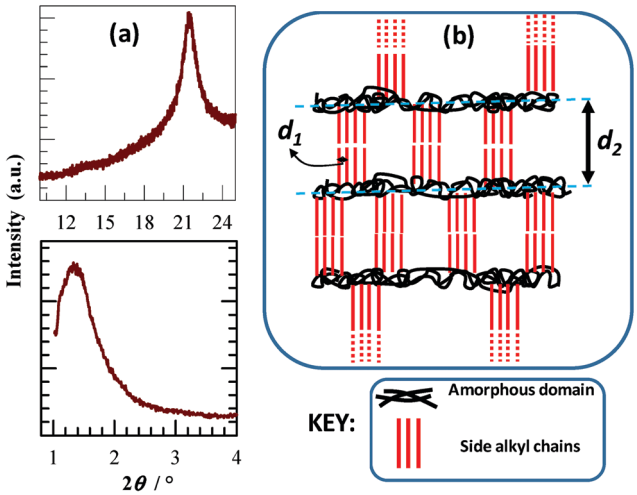

Fig. 2 (a) XRD pattern of a semicrystalline PAAc/C18A hydrogel specimen with 50 mol% C18A in the 10–25° and 1–4° 2θ ranges with scan rates of 1° min^{-1} and 0.5° min^{-1}, respectively. (b) Schematic illustration of crystalline and amorphous domains in semicrystalline hydrogels.

mechanical properties.[27–33] Later on, semicrystalline physical hydrogels without using any chemical cross-linker were prepared *via* bulk and micellar polymerization techniques.[34–36] These physical gels exhibit a high modulus (up to 300 MPa) and tensile strength (up to 7 MPa) and may sustain up to about 400% stretches. The blue triangles in Fig. 1 represent the mechanical parameters of a semicrystalline physical hydrogel prepared by bulk photopolymerization of *N*,*N*-dimethylacrylamide and *n*-octadecyl acrylate at a molar ratio of 70/30.[34] It is seen that such physical gels containing alkyl crystals belong to one of the groups of mechanically strong hydrogels. Further, they exhibit a highly efficient ability to self-heal as well as a shape-memory function with almost complete shape-fixity and shape-recovery ratios.[34–36] More recently, anisotropic mechanical properties were created in semicrystalline hydrogels mimicking the properties of many biological systems.[37,38]

The characteristic feature of semicrystalline physical hydrogels is that they undergo an abrupt and reversible change in their mechanical properties at the melting temperature of crystalline domains. Thus, in contrast to amorphous non-ionic hydrogels exhibiting a gradual softening with increasing temperature, semicrystalline physical gels rapidly change from a solid-like to a liquid-like state, opening up several applications such as shape-memory hydrogels, injectable gels, chemical motors, and smart inks for 3D or 4D printing. In this review, I present recent advances in the field of semicrystalline hydrogels by highlighting the physically cross-linked ones exhibiting self-healing and shape-memory functions together with anisotropic properties. Although semicrystalline hydrogels can also be prepared starting from polymers, *e.g.*, from aqueous polyvinyl alcohol solutions *via* freeze–thaw cycles,[39] this review covers those starting from hydrophilic and hydrophobic vinyl monomers.

2. Microstructure of crystalline zones in semicrystalline hydrogels

Plate and co-workers investigated the microstructure of alkyl crystals between long side alkyl chains of (meth)acrylates in dry and solution states and highlighted the importance of cooperative hydrophobic bonding to the polymer microstructure.[40–42] Formation of alkyl crystals is associated with partial alignment of the polymer chains in water making self-organization of their alkyl chains favorable.[43] Thus, it requires moderately flexible hydrophilic chains containing hydrophobic units with a side alkyl chain longer than 12 carbon atoms. Semicrystalline hydrogels typically exhibit two main XRD peaks at 2θ = 21.4°, and between 1.58 and 1.21°, revealing the existence of short- and long-range order (Fig. 2a).[21,24,31,44] The peak at 2θ = 21.4° is equivalent to a lattice spacing d_1 of 0.42 nm, indicating side-by-side arrangement of side alkyl chains, as schematically illustrated in Fig. 2b. The second diffraction peak appearing between 1.58 and 1.21° corresponds to a long spacing d_2 between 5.6 and 7.3 nm. This long spacing is close to twice the length of the alkyl side chain of hydrophobic units indicating tail-to-tail arrangement of side chains (Fig. 2b). Thus, the d_2 spacing increases from 5.6 to 7.3 nm as the side chain length increases from 18 to 22 carbon atoms, indicating formation of thicker bilayer structures in the hydrogels.[25]

Incorporation of carboxyl groups at the end of side alkyl chains significantly shortens the d_2-spacing and increases the melting temperature of the hydrogels, likely due to the H-bonding between carboxyl groups stabilizing the crystalline domains.[25] A similar observation was recently made by Wei and co-workers.[45] They showed that the critical alkyl chain length for the crystal formation decreases from 16 to 11 carbon atoms when a carboxylate group is incorporated at the terminal of the alkyl chain. Moreover, the water content of semicrystalline hydrogels is also an important parameter determining their crystalline structures.[24] Completely dried hydrogels exhibit no ordered structures whereas sharp XRD peaks appear in their wet states. As demonstrated by Osada and co-workers, a disorder-to-order transition in the hydrogels could be induced after addition of a small amount of water.[21,24] This transition is

due to the enhanced mobility of hydrophilic units of polymer chains in water facilitating side-by-side packing of alkyl chains. Conversely, an extensive amount of water in the hydrogels also destroys the crystalline order due to the high mobility of the network chains.[26] Thus, moderately flexible hydrophobically modified hydrophilic polymer chains in the presence of 10–50% water provide a suitable environment for the stability of alkyl crystals.

3. Effects of the synthesis parameters on the microstructure and mechanical properties of semicrystalline hydrogels

The properties of semicrystalline hydrogels prepared from hydrophilic and hydrophobic vinyl monomers *via* a free-radical mechanism strongly depend on the synthesis parameters, including the type and the amount of the monomers, the polymerization technique, the water content of the hydrogels and the presence of surfactants. The effects of these parameters are summarized in the following paragraphs. The hydrophobic monomers are abbreviated as C*x*y where *x* denotes the number of carbon atoms in the alkyl side chain, and y equals A and M for acrylate and methacrylate, respectively (Scheme 1). Because stearyl methacrylate (C17.3M) is composed of a mixture of *n*-hexadecyl- and *n*-octadecyl methacrylates, its average chain length of 17.3 is used in its short name. Further, the hydrophilic monomers that will be mainly discussed and their short names are acrylamide (AAm), acrylic acid (AAc), *N*,*N*-dimethylacrylamide (DMAA), *N*-isopropylacrylamide (NIPA), and *tert*-butylacrylamide (TBA), while the corresponding polymers are denoted by adding P before the monomer name (Scheme 1).

3.1. Effect of the hydrophobic monomer

Several *n*-alkyl (meth)acrylates with side alkyl chains ranging in length between 12 and 22 carbon atoms were used to investigate the effect of the hydrophobic monomer on the extent of intermolecular hydrophobic interactions in hydrogels.[46–48] Rheological measurements show that the loss factor $\tan\delta$ ($= G''/G'$, where G' and G'' are storage and loss moduli, respectively) decreases as the alkyl side chain length increases.[46] At a fixed side chain length, $\tan\delta$ also decreases by replacing the methacrylate backbone with the acrylate one. Because $\tan\delta$ is a measure of the energy dissipation in a material, this reveals that *n*-alkyl acrylates with a long alkyl side chain produce more elastic hydrogels than the corresponding methacrylates. In accord with this observation, the ultimate tensile strength of the hydrogels formed from hydrophobic acrylates is larger than those from methacrylates.[46]

At a low concentration of the hydrophobic monomer, *e.g.* at 2–5 mol% in the comonomer feed, physical hydrogels form *via* hydrophobic associations, whereas increasing the hydrophobe concentration above 20 mol% leads to the formation of hydrogels containing alkyl crystals.[27] Both the melting temperature T_m of the crystals and the degree of crystallinity f_{cry}, defined as the fraction of hydrophobic units in lamellar crystals, increase with increasing amount of the hydrophobic monomer. This behavior is illustrated in Fig. 3a for semicrystalline physical PDMAA/C17.3M, PDMAA/C18A, and PAAc/C18A hydrogels.[34] Both T_m and f_{cry} increase by replacing the C17.3M hydrophobe with the C18A one (curve 1 *vs.* 2 in Fig. 3a), likely due to the uniform length of the alkyl chains in C18A, and flexibility of acrylates as compared to methacrylates.[34] Moreover, when two hydrophobic monomers with different lengths of side chains are incorporated into the hydrogel, mixed crystalline domains are generated exhibiting a single T_m located between the T_ms of both hydrophobes.[25,31] The mechanical properties of semicrystalline

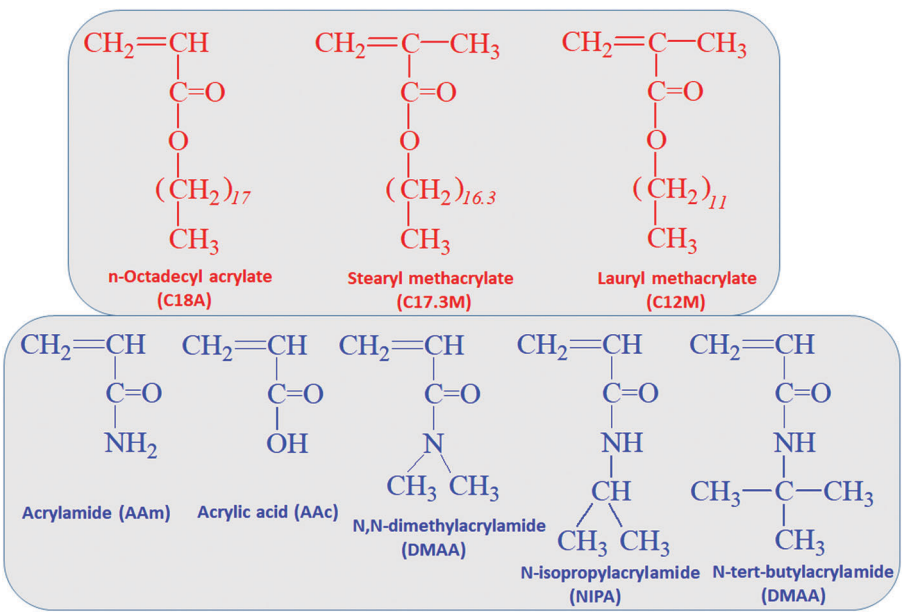

Scheme 1 Chemical structures of hydrophobic and hydrophilic monomers.

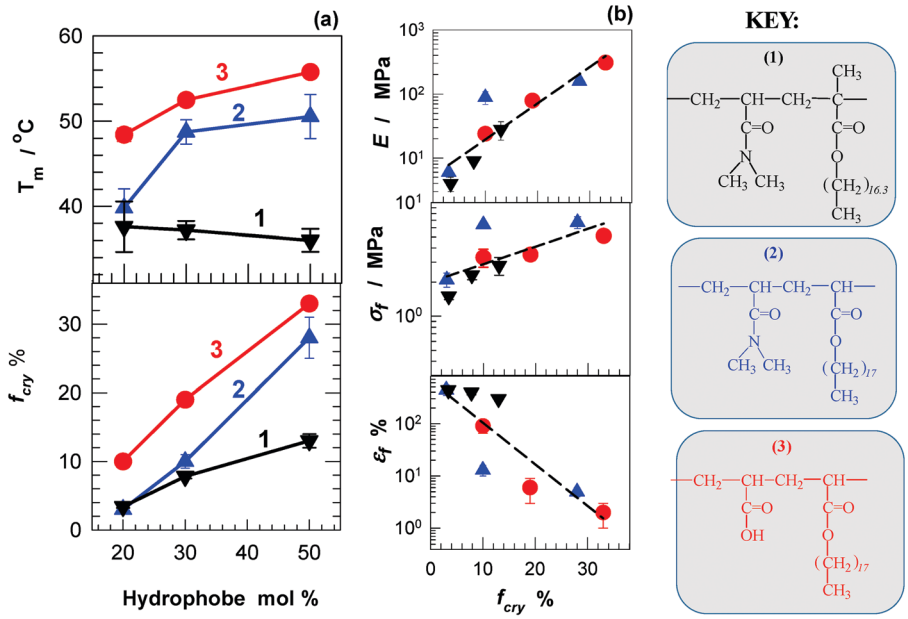

Fig. 3 (a) Melting temperature T_m, and the crystallinity f_{cry} of PDMAA/C17.3M (1), PDMA/C18A (2), and PAAc/C18A hydrogels (3) plotted against their hydrophobe contents. (b) Young's modulus E, tensile strength σ_f, and strain at failure ε_f of the hydrogels plotted against f_{cry}. The symbols are the same as in Fig. 1a. Strain rate ($\dot{\varepsilon}$) = 3.8 × 10^{-2} s^{-1}. The dashed lines are best fits to the experimental data. Fig. 3a and b were reprinted with permission from ref. 34. Copyright 2016 Elsevier Ltd.

hydrogels well correlate with the degree of crystallinity f_{cry} rather than the type of the hydrophobic monomers (Fig. 3b).[34] Both the Young's modulus E and tensile strength σ_f increase whereas strain to failure ε_ϕ decreases with increasing f_{cry}, indicating that semicrystalline hydrogels with a high crystallinity exhibit brittle behavior under tension. For instance, the modulus E of PAAc/C18A physical hydrogels increases from 24 to 310 MPa with increasing f_{cry} from 10 to 33%, whereas the stretch at break decreases from 91 to 2% (Fig. 3b).[34] As will be presented in Section 5, highly crystalline hydrogels can easily be made stretchable when a second hydrophobic unit with a short side alkyl chain is incorporated into the physical network.

The degree of crystallinity also affects the temperature sensitivity of semicrystalline hydrogels.[23] The magnitude of changes in their physical properties in response to a temperature change between below and above T_m increases significantly with increasing crystallinity f_{cry}. For instance, the physical PAAc/C18A hydrogel with 34% crystallinity has melting T_m and crystallization T_{cry} temperatures of 48 ± 2 °C and 43 ± 2 °C, respectively.[34–36] It undergoes a reversible 3 orders of magnitude change in the storage modulus G' between below and above these transition temperatures (Fig. 4). Thus, a weak gel above T_m exhibiting a modulus G' of 17 kPa and tan δ > 0.1 becomes a strong gel with G' = 18 MPa and tan δ close to 10^{-3} upon cooling below T_{cry}. Such a large difference in the modulus depending on the temperature and the physical nature of the cross-links are responsible for effective shape memory and self-healing functions of semicrystalline physical hydrogels.

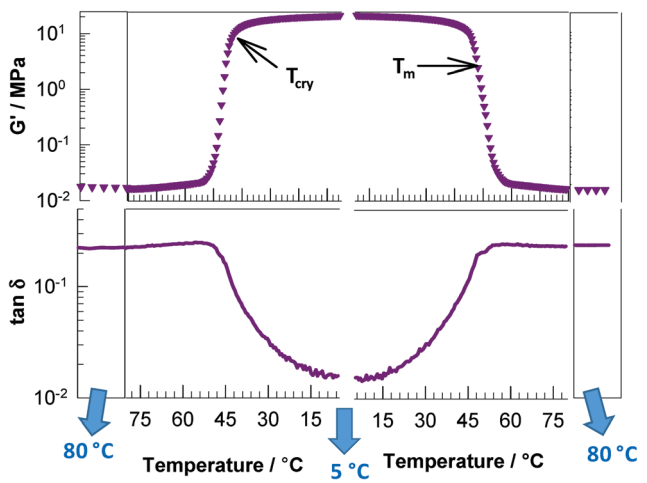

Fig. 4 G' and tan δ of a water-swollen PAAc/C18A physical gel specimen with 50 mol% C18A during a thermal cycle between 80 and 5 °C. Angular frequency ω = 6.28 rad s^{-1}. Strain amplitude γ_o = 0.1%.

3.2. Effect of the hydrophilic monomer

Bilici *et al.* conducted experiments using several hydrophilic monomers to find out the effect of the type of hydrophilic segments on the thermal stability of alkyl crystals.[31] Acrylic acid (AAc), acrylamide (AAm), *N*-isopropylacrylamide (NIPA), and *N*-*t*-butylacrylamide (TBA) were used in the gel preparation together with the hydrophobic monomer C18A at a fixed molar ratio of 65/35. The melting temperature T_m of the hydrogels increased in the order TBA < NIPA < AAm = AAc (41, 42, 53, and 53 °C, respectively).[31] The alignment of polymer chains and hence formation of lamellar crystals is apparently hindered by the bulky side groups of NIPA and TBA units in the hydrogels. Moreover, as compared to AAm, hydrogels derived from AAc exhibit drastic changes in the storage modulus in response to

temperature, which is attributed to the cooperative H-bonding between the carboxyl groups of AAc units facilitating crystal formation.[31] The H-bonding effect of the PAAc backbone to enhance crystal formation is also observable when one compares the PAAc backbone with the PDMAA one.[34] The former produces a higher melting temperature and a higher degree of crystallinity as compared to the latter backbone (see curve 3 *vs.* 2 in Fig. 3a). All these findings highlight the essential role of the hydrophilic backbone in the arrangement of alkyl chains in the hydrogels and AAc units are the best choice for the preparation of hydrogels containing the most stable crystals.

3.3. Effect of the water content

As discussed in Section 2, the water content of semicrystalline hydrogels affects significantly their crystallinity due to the fact that formation of lamellar crystals requires moderately flexible polymer chains that can be provided in an aqueous environment. Crystalline domains disappear after complete drying of the hydrogels or in the presence of an excess amount of water. The water content also affects the temperature-dependent changes in the mechanical properties of hydrogels. For instance, decreasing the water content of PAAc/C18A hydrogels with 35 mol% C18A from 75 to 46% increases the modulus G' at 25 °C from 8 to 15 MPa, which is accompanied by stronger variations of the dynamic moduli with temperature (Fig. 5a).[31]

3.4. Effect of the polymerization technique

Bulk copolymerization of hydrophilic and hydrophobic monomers in the presence of a radical initiator is a simple way to produce semicrystalline physical hydrogels as long as one of the monomers is in the liquid state at the polymerization temperature and the other monomer is soluble in it.[34,35] For instance, AAc and DMAA are liquids at room temperature and able to dissolve large amounts of C18A or C17.3M, so that their copolymerization can be conducted in the bulk state. Alternatively, solution polymerization in a common solvent, such as ethanol for the AAc/C18A comonomer pair, followed by replacing the organic solvent ethanol with water is also used for hydrogel preparation.[21] In recent years, the micellar polymerization technique has been preferred to prepare such hydrogels due to two main advantages: first, the presence of surfactant micelles in the gel network provides their melt-processability due to the weakening effect of surfactants on the crystalline region.[36] Second, this technique produces copolymers in a blocky structure in contrast to random copolymers formed by bulk or solution polymerization, leading to strong hydrophobic associations between the blocks of the hydrophobes.[49–53] This advantage of micellar polymerization is illustrated in Fig. 5b where the temperature responsivity of two PAAc/C18A gel specimens having the same composition and water content is compared.[31] One of the specimens, denoted as random, was prepared *via* solution polymerization in ethanol, whereas the other, denoted by block, was prepared *via* micellar polymerization followed by removing the surfactant by extracting with water. In contrast to the 120-fold change in G' of the hydrogel formed by random polymerization, that prepared *via* micellar polymerization exhibited a 1000-fold change in G' in response to a temperature change between below and above T_m.[31] This difference originates from the lower modulus and higher loss factor of the micellar gels above T_m due to the block-like structure of their copolymers. The following section reviews the micellar polymerization technique and its application to the preparation of melt-processable semicrystalline hydrogels.

4. Micellar polymerization and formation of semicrystalline micellar hydrogels

In the micellar polymerization technique developed by Candau and co-workers,[50,51,54–56] the hydrophobic monomer is first solubilized within the micelles and then copolymerized with a hydrophilic monomer in aqueous solutions by a free-radical mechanism. Because of the locally high concentration of the hydrophobic monomer within the micelles, the resulting hydrophilic polymers contain hydrophobic blocks creating strong hydrophobic associations in water. The number of units per

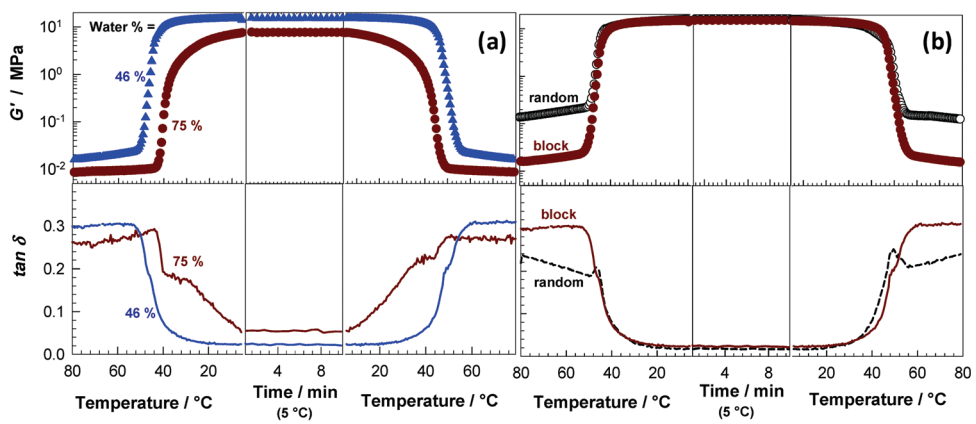

Fig. 5 Effects of the water content (a) and the polymerization technique (b) on the variations of G' and tan δ of PAAc/C18A hydrogels with 35 mol% C18A during a thermal cycle between 80 and 5 °C. ω = 6.28 rad s^{-1}. γ_o = 0.1%. Adapted with permission from ref. 31. Copyright 2013 American Chemical Society.

hydrophobic block, as well as the number of blocks per chain, can be tuned by the concentration of the reaction components. Sodium dodecyl sulfate (SDS) and cetyltrimethylammonium bromide (CTAB) are mainly used in the preparation of solutions or gels of hydrophobically modified hydrophilic polymers. The micellar polymerization technique is however limited to short hydrophobes, that is, to *n*-alkyl (meth)acrylates with a side alkyl chain length of less than 16 carbon atoms. For instance, although C12M can easily be solubilized in aqueous SDS solutions, larger hydrophobic monomers such as C8A or C22A are insoluble in SDS solutions because their alkyl chains are larger than the micellar size. Thus, the applicability of the micellar technique to the preparation of semicrystalline hydrogels requires solubilization of large hydrophobes in surfactant micelles.

This problem was recently solved by the addition of salts into aqueous solutions of ionic surfactants.[52,53] Because the addition of electrolytes suppresses the electrostatic interactions between ionic micelles, the micelles grow in size uniaxially to form several hundred nm long worm-like micelles (WLMs) having huge solubilization capacities for hydrophobic compounds (Fig. 6a).[52,53,57] The red curve in Fig. 6b shows the scattering profile of 243 mM SDS in 1 M NaCl solution obtained from small angle neutron scattering (SANS) measurements.[57] The slope of the $\ln[I\,q]$ *vs.* q^2 plot in the range of the scattering vector q = 0.06–0.19 Å^{-1} yields the cross-sectional radius of the structure as 1.76 nm, which is close to the extended length of the alkyl chain of SDS (1.67 nm), demonstrating uniaxial growth of monomeric SDS micelles, as also seen in the cryo-electron micrographs (Fig. 6a).[57] The growth of SDS micelles significantly enhances the solubilization of hydrophobic monomers such as C18A in SDS solutions (Fig. 6c).[31] In aqueous 22 w/v% SDS solution at 55 °C, the C18A solubility is only 0.1 w/v% whereas addition of 1.5 M NaCl to this solution increases the solubility of C18A to 16 w/v%.[31] At this C18A concentration, one may conduct the micellar copolymerization of C18A and AAc in an equimolar ratio at a total monomer concentration of 1 M to prepare semicrystalline hydrogels containing thermally stable crystal regions.

An interesting observation was that, after dissolving hydrophobic and hydrophilic monomers in aqueous WLM solutions, the solution viscosity drastically drops indicating disintegration of worm-like micelles, as evidenced from cryo-EM images.[57] This disintegration process can also be monitored by the SANS scattering curves (dark-cyan curve in Fig. 6b). The shape of the scattering curve after monomer addition can be fitted to monodisperse spheres with a radius of 2.4 nm revealing a conformation transition from worm-like to a spherical shape, as schematically illustrated in Scheme 2. This transition was attributed to the accumulation of the hydrophobes in the core of worm-like micelles, which increases the curvature of the micelle and hence facilitates a cylinder–sphere transition in the micellar shape.[57] The spherical shape of the micelles remains intact after conversion of the monomers to hydrophobically modified polymers whereas the micellar radius slightly increases from 2.4 to 2.8 nm (blue curve in Fig. 6b). Because the radius of the micellar core is determined by the fully extended length of the pendant alkyl tail, this increase reveals incorporation of hydrophobic units of the polymer into the micelles to form mixed micelles. As illustrated in Scheme 2, the mixed micelles composed of hydrophobic blocks of the polymer and alkyl tails of SDS act as junction zones by interconnecting hydrophilic blocks of the polymer chains in aqueous media to form a physical 3D network. Increasing the amount of the hydrophobic monomer in the feed above 20 mol% results in the formation of alkyl crystals within the mixed micelles. Due to the reversible nature of the micelles, semicrystalline micellar hydrogels thus formed exhibit almost complete self-healing efficiency.[36]

4.1. Effect of surfactants

Because surfactant micelles are effective in the solubilization of hydrophobic compounds, they also weaken hydrophobic interactions in hydrogels by dissolving hydrophobic association and crystalline regions to induce strong-to-weak gel, or gel-to-sol transitions.[36,52,53,58] Fig. 7a shows frequency sweep results of semicrystalline PAAc/C18A hydrogels with and without SDS, recorded at 25 and 65 °C, *i.e.*, at below T_{cry} and above T_m of alkyl

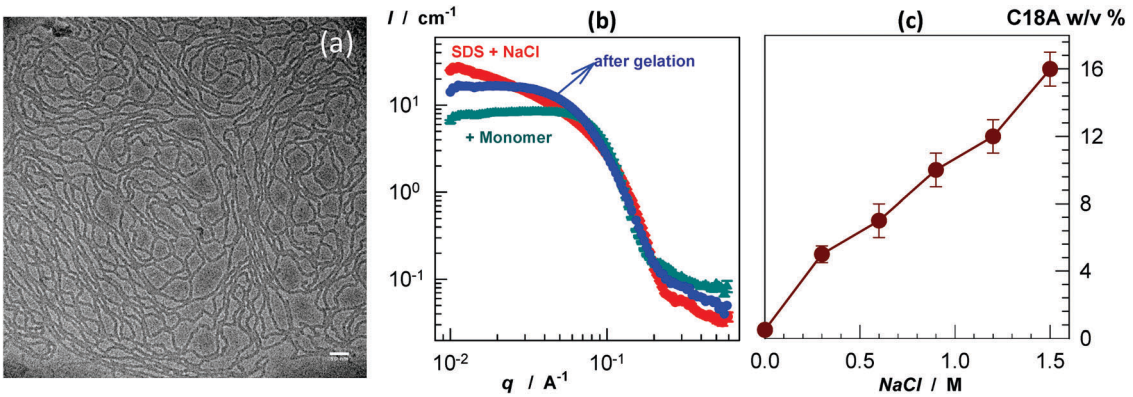

Fig. 6 (a) Cryo-electron micrograph of 243 mM SDS in 1 M NaCl solution after 1 : 10 dilution with 1 M NaCl. Scale bar = 50 nm. (b) SANS profiles for 243 mM SDS in 1 M NaCl before (red) and after (dark cyan) monomer addition, and after gelation (blue). Solvent = D_2O. (c) The solubility of C18A shown as a function of NaCl concentration. SDS = 22 w/v%. Temperature = 55 °C. Adapted with permissions from ref. 31 and 57. Copyright 2013, 2016 American Chemical Society.

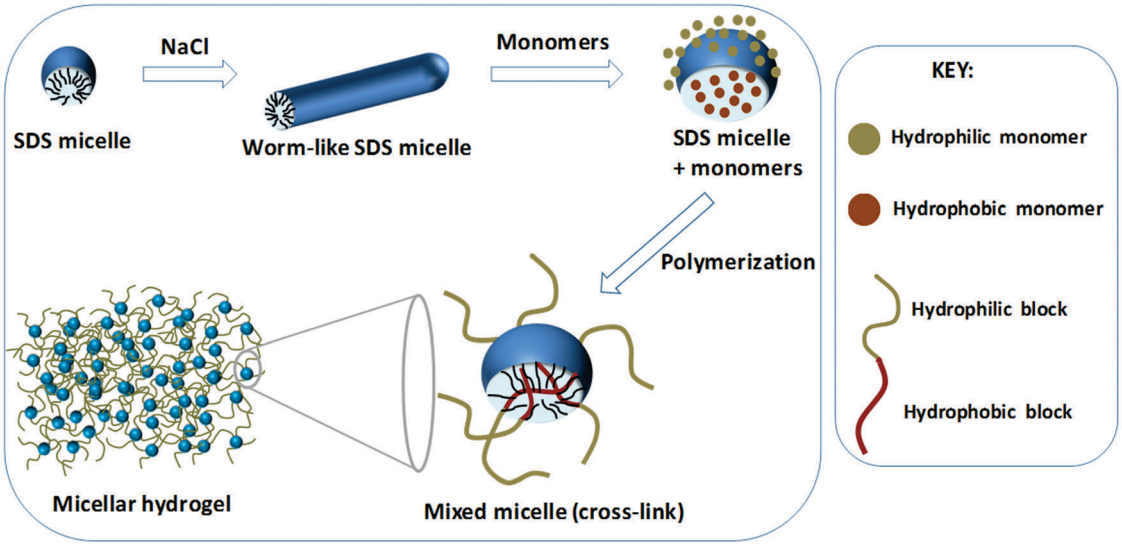

Scheme 2 Formation mechanism of micellar hydrogels *via* micellar polymerization in aqueous solutions of worm-like SDS micelles.

crystals, respectively.[36] Above T_m, the loss modulus G'' of the SDS-containing hydrogel is higher than the storage modulus G' at frequencies below 160 rad s^{-1}, revealing that it behaves as a semidilute polymer solution. Thus, surfactant micelles solubilize the associations and crystals to produce a polymer solution (Fig. 7b). Upon cooling below T_{cry}, the polymer solution transforms to a weak gel with a loss factor tan δ above 0.1, whereas removing SDS micelles from the physical network results in a strong gel with a frequency-independent G' of 8 MPa and a loss factor tan δ below 0.1.[36] Evidently, in the absence of surfactant micelles, the alkyl chains in associations and crystalline domains tend to attract each other more strongly to minimize their exposure to the hydrophilic gel phase than they do in the presence of surfactants, thereby the modulus increases and the loss factor decreases. Thus, a semidilute polymer solution can be converted to a mechanically strong hydrogel by a simple cooling/surfactant-removal procedure.

This feature of surfactant-containing semicrystalline physical gels enables their melt-processability and opens up several applications such as smart inks for 3D or 4D printing. For instance, when heated to 60 °C, SDS-containing PAAc/C18A gel specimens with 50 mol% C18A become a low viscosity liquid so they can be poured into molds of any permanent shape (Fig. 8a and b). Cooling the solution to room temperature followed by extraction of surfactant results in a mechanically strong gel with a predetermined shape. The gel has a shape-memory function due to the existence of alkyl crystals and associations between alkyl chains determining its temporary and permanent shapes, respectively. For instance, when a temporary "deformed-ring" shaped gel specimen is heated above T_m, it returns to its permanent ring shape within 15 s (Fig. 8c).[36] What is more, the gel has complete self-healing efficiency induced by heating the damaged region above T_m to melt alkyl crystals followed by cooling below T_{cry} to re-form the crystals between damaged surfaces (Fig. 8d). The key requirement for the existence of these three properties in a single hydrogel, namely melt-processability, shape-memory, and self-healing, is the extractability of surfactant micelles from the gel network. Thus, polyelectrolyte hydrogels and oppositely charged surfactant systems forming complexes cannot be used to create these features together.[59]

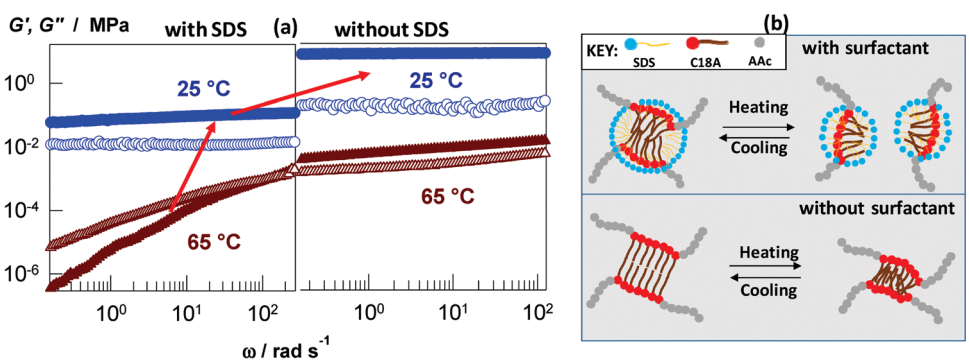

Fig. 7 (a) Frequency sweep results of PAAc/C18A hydrogels with (left) and without (right) SDS. G' and G'' are shown by the filled and open symbols, respectively. γ_o = 0.1%. C18A = 50 mol%. Temperature = 25 °C (circles) and 65 °C (triangles). (b) Schematic presentation of physical cross-links of the hydrogels with and without surfactant. Reprinted with permission from ref. 36. Copyright 2016 American Chemical Society.

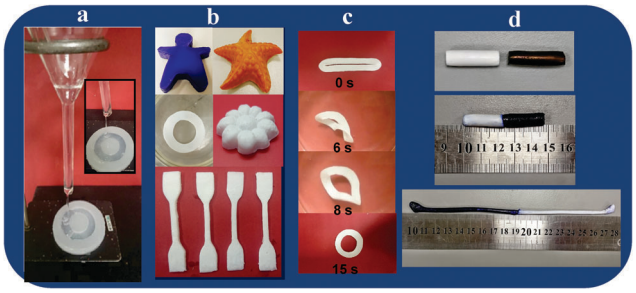

Fig. 8 Images of PAAc/C18A gel specimens showing their processability in the melt state at 60 °C (a and b), and self-healing and shape-memory functions (c and d). C18A = 50 mol%. For clarity, some of the gel specimens were colored. Reprinted with permission from ref. 36. Copyright 2016 American Chemical Society.

5. Mechanical properties of semicrystalline physical hydrogels

As seen in Fig. 1, semicrystalline physical hydrogels are one of the groups of mechanically strong hydrogels developed in the past two decades. At a high degree of crystallinity, they exhibit a high Young's modulus (up to 310 MPa) and sustain tensile stresses up to 7 MPa. However, they are brittle under tension and rupture at a few percent of elongation. To improve their tensile mechanical properties, the mixed-hydrophobe technique was recently developed which is based on the use of strong and weak hydrophobic monomers together in the gel preparation.[35]

For instance, the PDMAA/C18A hydrogel with 30 mol% C18A is brittle in tension with a fracture strain of 20% (dashed curve in Fig. 9a). However, when 0.2 mol% of its C18A units are replaced with the weak C12M hydrophobe, the hydrogel is no longer brittle and shows necking behavior (solid curve in Fig. 9a).[35] The addition of C12M does not affect the modulus E, and it remains almost unchanged, 71 ± 3 and 70 ± 5 MPa for 0 and 0.2% C12M, respectively, whereas the stretch at break

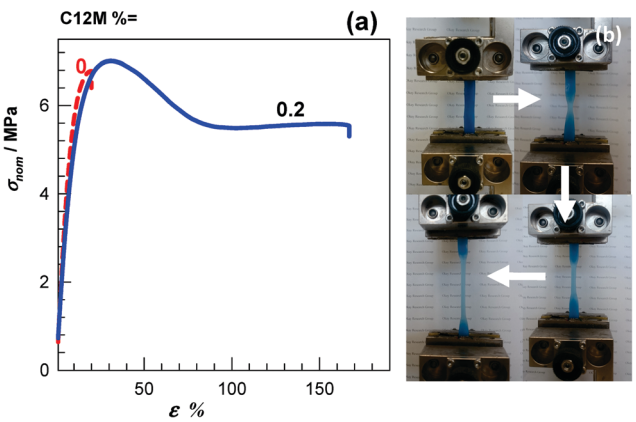

Fig. 9 (a) Nominal tensile stress (σ_{nom})–strain (ε) curves of semicrystalline PDMAA/C18A hydrogels. C12M contents are 0 (dashed curve) and 0.2 mol% (solid curve). Strain rate ($\dot{\varepsilon}$) = 8.3 × 10^{-2} s^{-1}. (b) Photographs taken during tensile testing of a C12M-containing gel specimen showing the appearance of necking behavior. Reprinted with permission from ref. 35. Copyright 2017 American Chemical Society.

increases 8-fold (from 20 to 167%) leading to a 10-fold increase in toughness (from 1.0 ± 0.2 to 9.6 ± 0.3 MJ m^{-3}). Similar results were also observed using several weak hydrophobes with a side alkyl chain length of less than 16 carbon atoms. This reveals that the inclusion of a small amount of a weak hydrophobe into the semicrystalline physical network induces a brittle-to-ductile transition without affecting its cross-link density. Uniaxial tensile tests conducted on PDMAA/C18A gel specimens with various C12M contents reveal the appearance of significant yielding between 0.1 and 2 mol% C12M (Fig. 10a).[35] The toughest hydrogel with the highest stretchability can be obtained at the lowest C12M level of 0.1 mol% (Fig. 10b).

WAXS and SAXS measurements conducted on the gel specimens indicate formation of layered lamellar crystals after incorporation of C12M segments into the hydrogels.[35] It was hypothesized that this structural change in the hydrogels upon C12M incorporation is responsible for their toughness improvement.[35] The proposed mechanism is schematically illustrated in Scheme 3, where red and black curves represent alkyl crystals and amorphous domains, respectively. Under an external force, the amorphous layer between alkyl crystals unfolds over time, while leaving behind lamellar clusters composed of several alkyl crystals separated by an amorphous backbone. The unfolded chains called tie molecules dissipate energy by transferring the external stress from one to another cluster, leading to deformation and finally fragmentation of the clusters at the yield point. The fragmentation of the clusters into smaller clusters and resulting energy dissipation are responsible for the toughness improvement of semicrystalline hydrogels. In the absence of C12M units, the lamellar clusters are not layered and hence tie molecules do not exist, resulting in a lack of energy dissipation and hence brittle behavior. The fact that the stress–strain curves of the hydrogels with or without C12M are similar up to the yield point also supports this mechanism (Fig. 3, 9a and 10a). At the yield point, the hydrogel without C12M fractures in a brittle fashion whereas that with C12M exhibits necking behavior indicating internal damage due to the fragmentation of lamellar clusters. Calculations using the lamellar cluster model of Nitta and co-workers reveal that the clusters are fragmented into single polymer chains at the yield point.[35,60,61]

The energy dissipation mechanism discussed above is similar to that of double-network (DN) hydrogels developed by Gong and co-workers.[10,62] DN hydrogels are composed of two interpenetrated and interconnected networks. The first brittle network breaks into smaller clusters at the yield point by dissipating energy whereas the second ductile network keeps the macroscopic sample together. This energy dissipation mechanism arising from the sacrificial covalent bonds of the first network results in extraordinary mechanical properties.[10,62] In the case of semicrystalline hydrogels, instead of the first network, lamellar clusters break under stress and hence dissipate energy whereas amorphous domains keep the sample together. The distinct advantage of lamellar crystals is their reversible nature as compared to the irreversible bonds of the first network in DNs. After fragmentation of the lamellar clusters into smaller ones, they can be repaired by simply heating above T_m and subsequently cooling to room temperature.

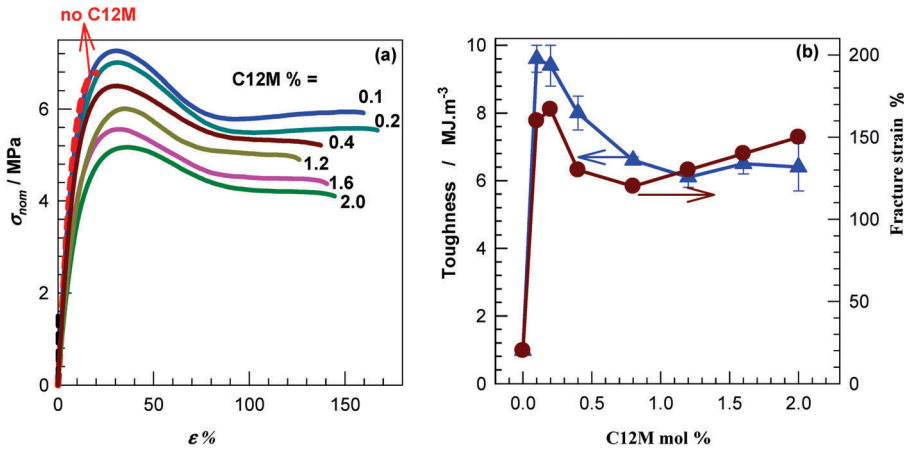

Fig. 10 (a) Tensile stress–strain curves of PDMAA/C18A hydrogels with various C12M contents as indicated. C18A mol% = 30 − C12M mol%. $\dot{\varepsilon} = 8.3 \times 10^{-2}$ s^{-1}. (b) Toughness and fracture strain of the hydrogels plotted against C12M mol%. Adapted with permission from ref. 35. Copyright 2017 American Chemical Society.

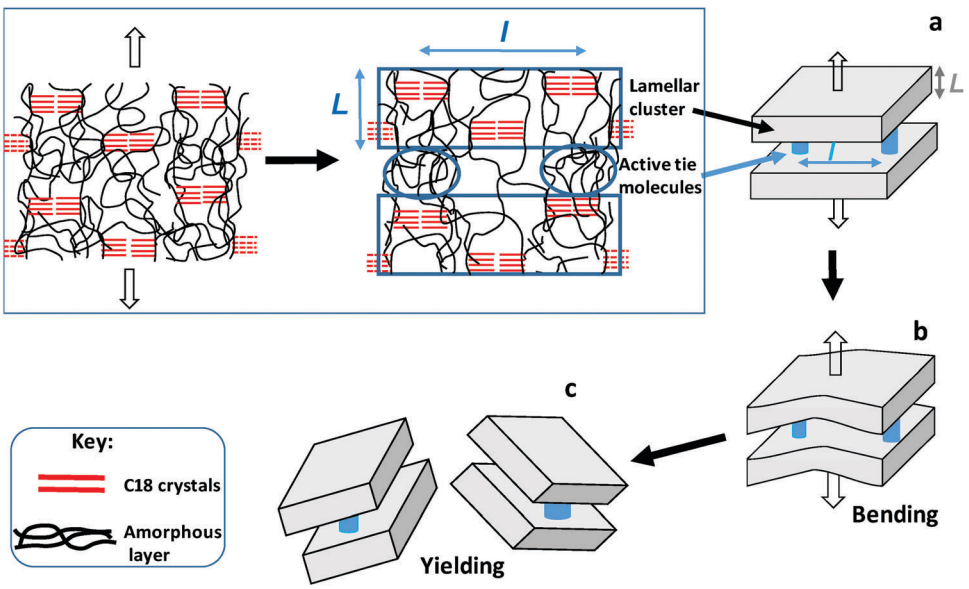

Scheme 3 Schematic illustration of the mechanism of toughness improvement *via* the mixed-hydrophobe technique. Layered lamellar clusters, indicated in rectangles, are formed upon incorporation of C12M segments into semicrystalline hydrogels and they are interconnected by active tie molecules (a). Lamellar clusters deform under stress (b) and finally, break at the yield point (c). Reprinted with permission from ref. 35. Copyright 2017 American Chemical Society.

This distinct difference between DNs and semicrystalline hydrogels was demonstrated by successive tensile cycles up to a strain below the fracture point (Fig. 11).[35] When a DN hydrogel is subjected to two successive cycles, the virgin specimen exhibits a distinctive yield point during the first loading at which the brittle first-network starts to break up by dissipating energy (Fig. 11a). Because of the covalent nature of its bonds, it is irreversibly broken so that the second loading curve exhibits no yield point and hence both the modulus and toughness significantly decrease as compared to those of the first loading (Fig. 11a).[35] This irreversibility is the main disadvantage of the classical DN hydrogels. Similar to DNs, the second loading curve of semicrystalline hydrogels follows a different path to the first loading due to the damage done to the lamellar crystals (Fig. 11b). As a consequence, the modulus significantly decreases and the yield behavior vanishes after the first loading (Fig. 11c). However, heating the gel specimen at 70 °C to melt the alkyl crystals and then cooling to room temperature before the second loading results in almost complete recovery of the virgin stress–strain curve (the dashed curve in Fig. 11b). 93% of both modulus and yield stress could be recovered after the heating/cooling procedure (Fig. 11c).[35]

6. Semicrystalline hydrogels with anisotropic mechanical properties

One of the major challenges in the field of tough and soft materials is to create anisotropic mechanical properties as observed in many biological systems.[63] Several techniques have

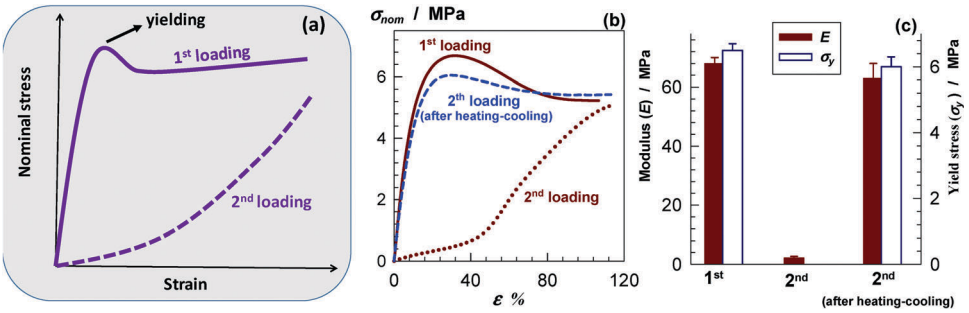

Fig. 11 (a) Scheme showing two successive loading curves before the fracture of a classical DN gel specimen. (b) Two successive loading curves up to a 100% stretch ratio for a PDMAA/C18A gel specimen. C12M = 0.4 mol%. $\dot{\varepsilon} = 8.3 \times 10^{-2}$ s^{-1}. The second loading was carried out without (dotted curve) and with (dashed curve) the heating/cooling treatment of the gel specimen. (c) Young's modulus E and yield stress σ_y of the same gel specimen calculated from the loading curves given in (b). Reprinted with permission from ref. 35. Copyright 2017 American Chemical Society.

been developed in the past years to achieve this aim, including the directional freezing technique,[64,65] and stress- or ion-diffusion-induced alignment of the network chains followed by fixing the oriented chains by post-polymerization.[66–73] In this respect, semicrystalline hydrogels are a good candidate to produce mechanically strong hydrogels with anisotropic properties. To create anisotropy, they are first heated above T_m to melt their crystalline domains so that they become weak and can easily be stretched to a predetermined prestretch ratio λ_o (Fig. 12a).[37] Cooling the prestretched hydrogels below T_m results in the fixation of the stretched chain conformation due to the re-formation of alkyl crystals. The prestretch ratio λ_o determines the extent of microstructural and mechanical anisotropy as well as the mechanical properties parallel ($\parallel$) and perpendicular ($\perp$) to the prestretching direction.[37]

It was shown that the degree of crystallinity f_{cry} increases and the equilibrium swelling ratio q_w in water decreases with increasing λ_o up to around λ_o = 1.8 for PDMAA/C18A physical hydrogels with 30 mol% C18A (Fig. 12b).[37] This reveals strain-induced crystallization of non-associated side alkyl chains, forming additional physical cross-links and hence reducing the swelling capacity. The opposite behavior appears at higher prestretch ratios; f_{cry} decreases and q_w increases with increasing λ_o up to 8 suggesting disruption of lamellar crystals (Fig. 12b). WAXS and SAXS patterns of the hydrogels show that the lamellar crystals increasingly align parallel to the stretching direction up to around λ_o = 1.8, while those in the perpendicular direction become more disordered.[37] The reverse behavior appears above this critical prestretch ratio; the alignment increases in the direction perpendicular to the prestretching direction with increasing λ_o while the crystals in the parallel direction become more disordered.

The microstructural changes in semicrystalline hydrogels depending on the prestretch ratio well correlate with their mechanical properties.[37] Except for the non-prestretched gel specimen, all prestretched PAAc/C18A specimens display mechanical anisotropy (Fig. 13a). In accord with the swelling and crystallinity results, they exhibit different λ_o-dependences below and above the critical prestretch ratio $\lambda_{o,c}$ = 1.8:[37]

$\lambda < \lambda_{o,c}$: along the parallel direction, the non-prestretched brittle gel becomes a ductile one after prestretching and its toughness further increases with increasing λ_o. The brittle-to-ductile transition occurs at the lowest λ_o of 1.2. Along the opposite direction, the non-prestretched gel still remains brittle over the whole range of λ_o.

$\lambda > \lambda_{o,c}$: the mechanical properties in the parallel direction deteriorate as λ_o is increased while a significant toughness improvement appears in the opposite direction.

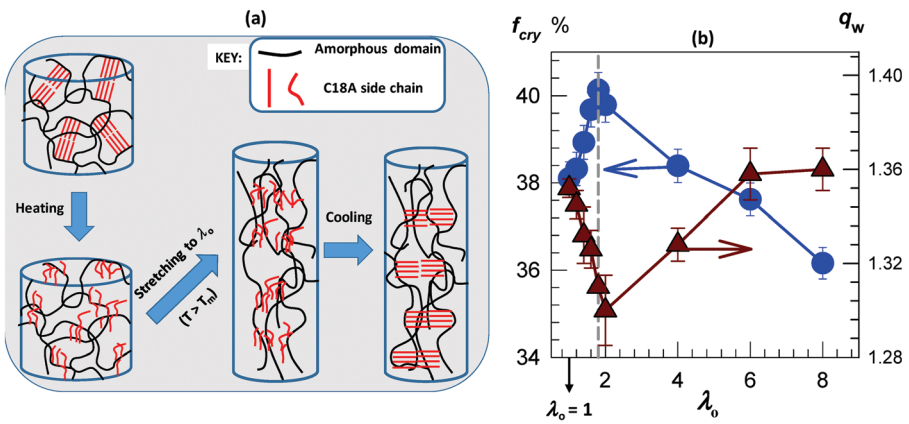

Fig. 12 (a) Scheme showing the prestretching technique to create anisotropic mechanical properties in semicrystalline hydrogels. (b) The prestretch ratio λ_o dependences of the weight swelling ratio q_w and the crystallinity degree f_{cry} of PDMAA/C18A hydrogels. C18A = 30 mol%.

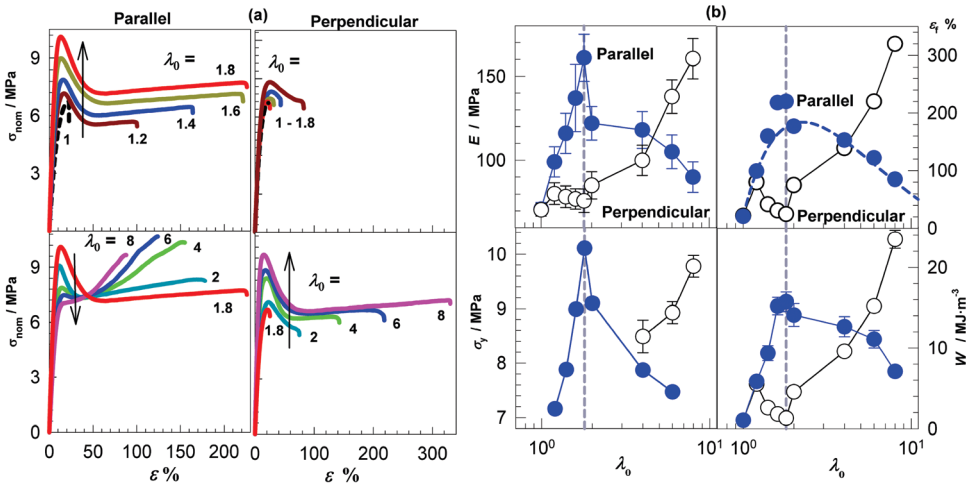

Fig. 13 (a) Tensile stress–strain curves of PAAc/C18A hydrogels with various prestretch ratios λ_o. C18A = 30 mol%. The tensile data were recorded in directions parallel (∥) and perpendicular (⊥) to the prestretching. Strain rate: 5 min^{-1}. (b) Young's modulus E, yield stress σ_y, strain at break ε_f, and toughness W of the hydrogels plotted against λ_o. The data were from directions parallel (filled symbols) and perpendicular (open symbols) to the prestretching. The vertical dashed line represents $\lambda_{o,c}$ = 1.8. Reprinted with permission from ref. 37. Copyright 2018 Elsevier Ltd.

The opposite effect of λ_o at below and above $\lambda_{o,c}$ = 1.8 on the mechanical properties is also observable in λ_o-dependent variations of Young's modulus E, yield stress σ_y, strain at failure ε_f, and toughness W of the hydrogels measured in both directions (Fig. 13b).[37] All the mechanical parameters attain their maximum values at the critical prestretch ratio $\lambda_{o,c}$, when measured in the parallel direction, whereas those measured in the vertical direction start to increase later, *i.e.*, after passing the $\lambda_{o,c}$ ratio. As a consequence, hydrogels with a maximum degree of mechanical anisotropy could be prepared at a prestretching of $\lambda_{o,c}$. For instance, the hydrogel at $\lambda_{o,c}$ has Young's moduli of 161 ± 14 and 76 ± 7 MPa, and a stretch at break of 220 and 25%, in parallel and perpendicular directions, respectively. In terms of the mechanical anisotropy defined as the ratio of a mechanical property in two perpendicular directions, the anisotropies in modulus and toughness at $\lambda_{o,c}$ are 2.1 ± 0.2 and 12 ± 1, respectively.[37]

The above findings could be explained with the alignment of the lamellar clusters to the prestretching direction. By the mixed-hydrophobe technique described in the previous section, this alignment was achieved by the addition of a weak hydrophobic monomer (Fig. 10). Prestretching of the hydrogels increases the thickness of the lamellar clusters in the parallel direction so that a higher external force is needed for their fragmentation. This leads to increasing modulus and toughness of the hydrogels in the parallel direction with increasing λ_o. In the opposite direction, however, because tie molecules are pulled away from the lamellar clusters, thinner and weaker clusters form leading to a brittle behavior. Calculations show that the tie molecules interconnecting lamellar clusters are in the flexible regime at λ_o below $\lambda_{o,c}$ whereas at larger values of λ_o, the maximum extension of tie molecules is reached revealing that $\lambda_{o,c}$ corresponds to the limited extensibility of tie molecules.[37]

7. Self-healing and shape-memory functions of semicrystalline hydrogels

Melting of the physical cross-links in semicrystalline hydrogels and their reformation upon cooling necessarily result in a self-healing ability induced by heating the damaged zones (Fig. 8d). Healing in such hydrogels is generally induced by first heating the cut surfaces above T_m and then pushing the surfaces together for a certain time followed by cooling to room temperature. It was recently shown that, instead of external heating, internal heating generated by light can also be used to self-heal semicrystalline hydrogels.[74] By including a small amount of gold nanoparticles in the hydrogels as the internal heating source, Zhang and co-workers demonstrated self-healing in PDMAA/C18A hydrogels induced by laser light of a wavelength close to the surface plasmon resonance (SPR) of the particles.[74] Heat generated by gold particles due to SPR increases the temperature of the damaged zone leading to the melting of alkyl crystals. After turning the laser off, the crystals formed again bind the fractured surfaces with a high healing efficiency.

Because the alkyl crystals at the surfaces melt upon external or internal heating to produce non-associated side alkyl chains, the free chains thus formed orient away from the water-containing, hydrophilic bulk gel phase toward the cut surfaces in contact with air. This phenomenon is similar to that of surfactants at water–air interfaces whose alkyl chains orient at the surface. After pressing the surfaces together and then cooling below T_m, alkyl side chains on both surfaces organize to form alkyl crystals at the interface to decrease their exposure to the gel phase leading to the healing of the hydrogels. Fig. 14 shows the modulus E, compressive fracture strength σ_f and strain at break ε_f of virgin physical PAAc/C18A hydrogels (filled symbols) together with the healed ones at 80 °C for 24 h (open symbols) plotted against the C18A content.[36] High strength

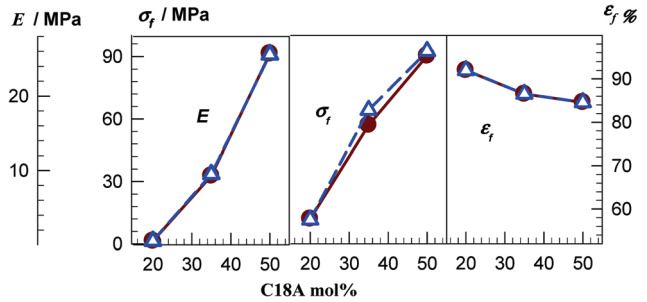

Fig. 14 Variations of E, σ_f, and ε_f of semicrystalline PAAc/C18A hydrogels with their C18A contents. Filled and open symbols represent the data of virgin and healed gel specimens, respectively. Reprinted with permission from ref. 36. Copyright 2016 Elsevier Ltd.

hydrogels with a modulus of 0.5–26 MPa and compressive stress of 12–90 MPa can completely be healed using the heating/cooling treatment.

Self-healing behavior was also reported in hybrid semicrystalline hydrogels consisting of hard and soft components interconnected with a strong interface.[38] Such hybrids mimicking biological systems like intervertebral discs, tendon–bone systems with enthesis junctions, are important materials in biological applications.[75–79] They were prepared by stratification of hydrophilic/hydrophobic monomer solutions having different densities followed by photopolymerization of the stratified solutions.[38] Fig. 15a1 shows the image of a dumbbell-shaped hybrid semicrystalline hydrogel specimen composed of PDMAA/C18A and PDMAA/C17.3M components, denoted as C1 and C2, respectively. C1 has a higher melting temperature compared to C2 (48 °C *vs.* 35 °C) and they are interconnected by an interface region indicated by the yellow arrow. The interface is mechanically stronger than both gel zones so that under stress, the interface remains intact whereas the hybrid breaks at one of the gel zones.[38] On cutting the gel specimen at both gel zones into three parts and subjecting them to the heating/cooling treatment for 1 h, they merge into a single gel specimen (Fig. 15a2 and a3). Tensile stress–strain curves of healed (dashed curve) and virgin C1/C2 hydrogels are shown in Fig. 15b. It is seen that the ultimate mechanical properties of the virgin gel significantly reduce after cutting at both gel zones. This is due to the fact that the sample breaks at the cut region created in the C1 component which is relatively brittle.[38] However, when the hybrid gel specimen is cut at the C2 site, it exhibits yielding and around 70% healing efficiency after the heating-induced healing process. Replacing the C2 component with the non-crystalline, stretchable PDMAA/C12M hydrogel denoted as C3, the resulting C1/C3 hybrid exhibits more than 80% healing efficiency independent of the location of the cuts (Fig. 15c).[38]

In addition to self-healing, semicrystalline hydrogels exhibit a shape-memory function due to the existence of two types of cross-links (Fig. 8c).[21–23,29,44,45] Upon heating above T_m and deforming the gel specimen to a temporary shape, followed by cooling below T_m, the temporary shape is fixed by alkyl crystals acting as switching segments. To recover the permanent shape, the specimen is again heated above T_m to melt the crystals and hence to induce a conformation transition in the polymer chains from elongated to the entropically most favored configuration of random coils. The resulting permanent shape of the specimen is determined by hydrophobic associations acting as netpoints. Dipole–dipole interactions have also been

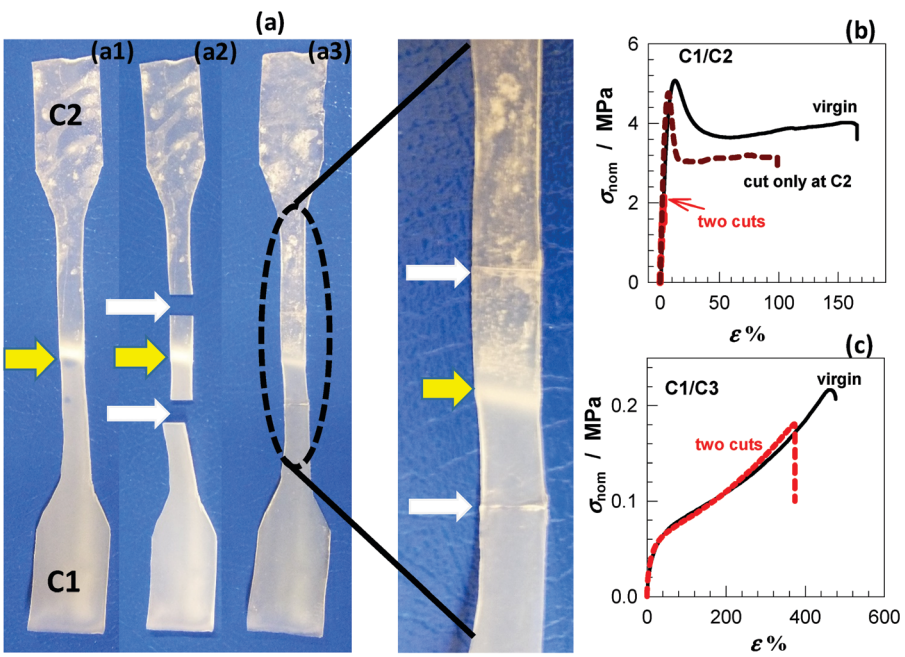

Fig. 15 (a) Photographs of a dumbbell-shaped C1/C2 hydrogel sample before and after cutting, and after healing. The interface of the gel zones and the cut regions are indicated by yellow and white arrows, respectively. (b and c) Tensile stress–strain curves of C1/C2 (b) and C1/C3 hybrids demonstrating their self-healing behavior. Reprinted with permission from ref. 38. Copyright 2018 American Chemical Society.

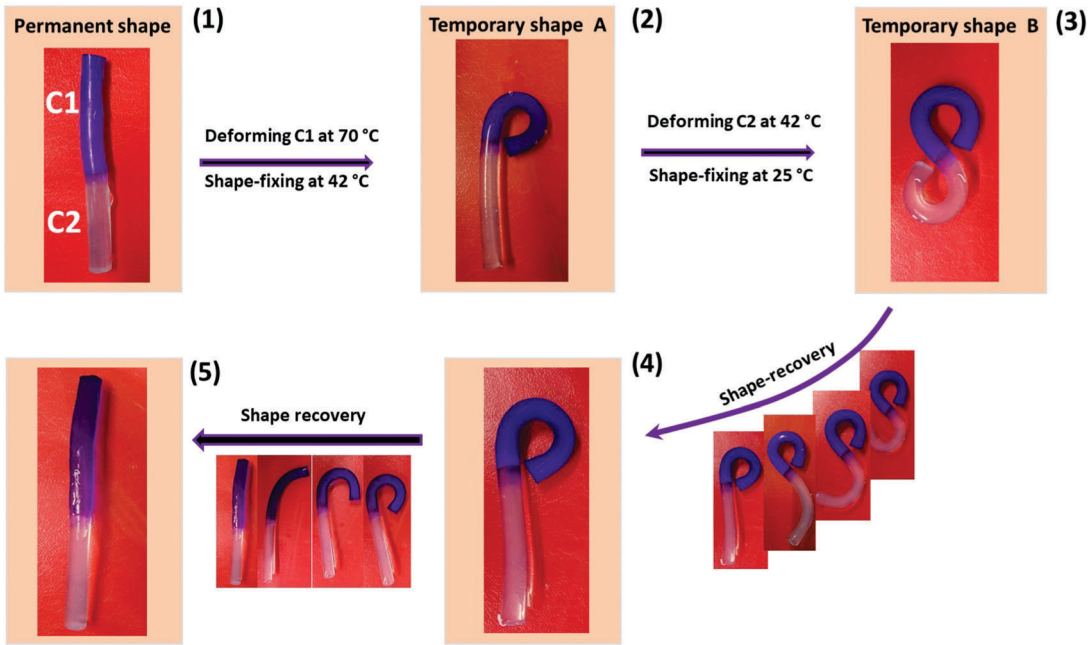

Fig. 16 Photographs of a C1/C2 hybrid gel specimen showing its pseudo triple-shape-memory behavior. Images labeled by 1, 2, and 3 illustrate its permanent shape, and temporary shapes A and B, respectively. Successive recoveries of the temporary shape-A and permanent shape at 42 and 70 °C, respectively, are shown by images 4 and 5. Reprinted with permission from ref. 38. Copyright 2018 American Chemical Society.

used to trigger the shape-memory function of the hydrogels.[33] The association and dissociation of cyano groups in the hydrogels in response to zinc ions enable them to memorize the temporary shape and recover to the permanent shape.[33]

The shape-memory behavior of hydrogels can be quantified in terms of the strain recovery R_r and strain fixity R_f ratios which are determined by thermomechanical shape-memory cycles.[80] The shape fixity ratio R_f of semicrystalline physical hydrogels discussed above is above 99%, revealing that they almost completely preserve their temporary shapes after cooling below T_m.[36] Moreover, after subjecting the specimens to a preconditioning cycle before the tests, the shape recovery ratio R_r is around 97% in 4 successive cycles revealing excellent reversibility of the shape changes of semicrystalline physical hydrogels.[36] It was shown that hydrogels having crystallizable poly(e-caprolactone) acting both as a cross-linker and switching segments have heating-triggered shape-memory behavior with shape-fixity and recovery ratios up to 100%.[30]

Because hybrid hydrogels consisting of C1 and C2 components have two melting temperatures in their domains, namely 48 and 35 °C in C1 and C2 zones, respectively, they can remember two temporary shapes, which is called the triple-shape memory effect (Fig. 16).[81] The C1/C2 hybrid gel specimen is first heated above both T_ms and its C1 zone is deformed. When the specimen is cooled between the two T_ms of its components, the first temporary shape (A) is fixed due to the formation of alkyl crystals in the C1 zone (image 2). The still melted C2 zone is then deformed into a second temporary shape (B) which is fixed by cooling below both T_ms. For the shape recovery, the specimen is first heated between the two T_ms to recover the first temporary shape whereas further heating above both T_ms recovers the permanent shape (images 4 and 5).

8. Conclusions and outlook

Semicrystalline physical hydrogels belong to one of the groups of mechanically strong hydrogels. In this review article, recent advances in the field of semicrystalline hydrogels prepared from hydrophilic and hydrophobic vinyl monomers *via* a free-radical mechanism were summarized by highlighting the physically cross-linked ones. Semicrystalline physical hydrogels are mainly prepared by bulk, solution, or micellar polymerization of a hydrophilic monomer with *n*-alkyl (meth)acrylates with side alkyl chains ranging in length between 16 and 22 carbon atoms. As compared to bulk or solution polymerization techniques, micellar polymerization has two main advantages: first, the presence of surfactant micelles in semicrystalline hydrogels provides their melt-processability due to the weakening effect of surfactants on the crystalline region. The second advantage of the micellar technique is formation of copolymers in a blocky structure in contrast to random copolymers formed by bulk or solution polymerization facilitating formation of stronger hydrophobic associations.

The hydrogels typically exhibit both short- and long-range order due to the side-by-side and tail-to-tail arrangements of side alkyl chains, with *d*-spacings of 0.42 and 5.6–7.3 nm, respectively. The nano-sized alkyl crystals in semicrystalline hydrogels contribute significantly to their mechanical properties. One might think that the alkyl crystals in the hydrogels are similar to the β-sheets in silk fibroin responsible for its high

strength and toughness.[82] The long-range order in semicrystalline hydrogels can be varied by changing the length of side alkyl chains and the water content of the hydrogels, as well as by incorporation of a carboxyl group at the end of the side chain.

The properties of semicrystalline physical hydrogels strongly depend on the synthesis parameters, including the type and the amount of the monomers, the polymerization technique, the water content of the hydrogels and the presence of surfactants. At a low concentration of the hydrophobic monomer, physical hydrogels form *via* hydrophobic associations whereas increasing the hydrophobe concentration above 20 mol% leads to the formation of hydrogels containing crystalline domains. Both the melting temperature T_m of the crystals and the degree of crystallinity f_{cry} increase with an increasing amount of the hydrophobic monomer. The mechanical properties of semicrystalline hydrogels correlate with the crystallinity f_{cry} rather than the type of the hydrophobic monomers. Both the Young's modulus E and tensile strength σ_f increase whereas strain to failure ε_f decreases with increasing f_{cry} indicating that semicrystalline hydrogels with high crystallinity exhibit brittle behavior under tension. The degree of crystallinity also affects the temperature sensitivity of semicrystalline hydrogels. At a high degree of crystallinity, a semicrystalline hydrogel undergoes a reversible 3 orders of magnitude change in the storage modulus G' between below and above the transition temperature. Although hydrogels with a high degree of crystallinity exhibit brittle behavior under tension, their tensile mechanical properties can easily be improved by the mixed-hydrophobe technique. The inclusion of a small amount of a weak hydrophobe such as C12M in a semicrystalline physical network induces a brittle-to-ductile transition without affecting its cross-link density.

Melting of alkyl crystals in semicrystalline hydrogels and their recrystallization upon cooling result in a self-healing ability induced by external or internal heating of the damaged zones. It was shown that high strength semicrystalline hydrogels with a modulus of 0.5–26 MPa and compressive stress of 12–90 MPa can be completely healed using the heating/cooling treatment. In addition to self-healing, semicrystalline hydrogels exhibit a shape-memory function triggered by heating due to the existence of two types of cross-links, namely alkyl crystals and hydrophobic associations acting as switching segments and netpoints, respectively. The shape fixity and recovery ratios of semicrystalline physical hydrogels are 97–99%, revealing that they almost completely preserve their temporary shapes and exhibit excellent reversibility of the shape changes. Because hybrid hydrogels consisting of two semicrystalline gel components have two different melting temperatures in their domains, they also exhibit a pseudo triple-shape memory effect.

The extraordinary mechanical performance as well as self-healing and shape-memory functions of semicrystalline physical hydrogels with tailorable properties can extend the application areas of shape-memory materials enormously to load-bearing applications. The trends reveal that shape-memory semicrystalline hydrogels with various external trigger methods can be developed for advanced biomedical and biological applications. The melt-processability of semicrystalline physical hydrogels prepared by micellar polymerization can open up several new applications such as injectable hydrogels, and smart inks for 3D or 4D printing. Further, semicrystalline hydrogels with anisotropic properties mimicking many biological systems have use as biomaterials, artificial organs and prosthetic devices. For instance, biological tissues such as bone, cartilage, ligaments, tendons and intervertebral discs (IVD) are mainly composed of hard and soft components with an extremely tough interface. Tendons are joined to bone through a strong interface known as the enthesis. IVD providing dissipation of energy, load transfer and flexibility to the spine are composed of hard and soft components integrated into a single fused material. Interfacing soft materials with large mismatches in the mechanical properties to mimic biological systems is a challenging area of research. The initial studies in this field, as summarized in Section 3, reveal that semicrystalline physical hydrogels are a good candidate to produce multi-segmented, biocompatible soft materials with self-healing and shape memory functions.

Conflicts of interest

There are no conflicts of interest to declare.

Acknowledgements

This work was supported by Istanbul Technical University, BAP TDK-2017-40506. The author also thanks Turkish Academy of Sciences (TUBA), full member 2018, for the partial support.

Notes and references

1 P. Calvert, *Adv. Mater.*, 2009, **21**, 743–756.
2 E. Calo and V. V. Khutoryanskiy, *Eur. Polym. J.*, 2015, **65**, 252–267.
3 K. H. Bae, L.-S. Wanga and M. Kurisawa, *J. Mater. Chem. B*, 2013, **1**, 5371–5388.
4 S. J. Buwaldaa, K. W. M. Boerea, P. J. Dijkstrab, J. Feijenc, T. Vermondena and W. E. Henninka, *J. Controlled Release*, 2014, **190**, 254–273.
5 *Supramolecular polymer networks and gels, Book series*, ed. S. Seiffert, Advances in Polymer Science, Springer, Berlin, Germany, 2015.
6 B. Q. Y. Chan, Z. W. K. Low, S. J. W. Heng, S. Y. Chan, C. Owh and X. J. Loh, *ACS Appl. Mater. Interfaces*, 2016, **8**, 10070–10087.
7 C. Creton, *Macromolecules*, 2017, **50**, 8297–8316.
8 J. Fu, *J. Polym. Sci., Part B: Polym. Phys.*, 2018, **56**, 1336–1350.
9 Y. Liu and S. Hsu, *Front. Chem.*, 2018, **6**, 449.
10 J. P. Gong, Y. Katsuyama, T. Kurokawa and Y. Osada, *Adv. Mater.*, 2013, **15**, 1155–1158.
11 Q. Chen, D. Wei, H. Chen, L. Zhu, C. Jiao, G. Liu, L. Huang, J. Yang, L. Wang and J. Zheng, *Macromolecules*, 2015, **48**, 8003–8010.

12 J. Li, Z. Suo and J. J. Vlassak, *J. Mater. Chem. B*, 2014, **2**, 6708–6713.
13 J.-Y. Sun, X. Zhao, W. R. K. Illeperuma, O. Chaudhuri, K. H. Oh, D. J. Mooney, J. J. Vlassak and Z. Suo, *Nature*, 2012, **489**, 133–136.
14 L. Zhang, J. Zhao, J. Zhu, C. He and H. Wang, *Soft Matter*, 2012, **8**, 10439–10447.
15 K. Haraguchi and T. Takehisa, *Adv. Mater.*, 2002, **14**, 1120–1124.
16 T. L. Sun, T. Kurokawa, S. Kuroda, A. B. Ihsan, T. Akasaki, K. Sato, M. A. Haque, T. Nakajima and J. P. Gong, *Nat. Mater.*, 2013, **12**, 932–937.
17 X. Hu, M. Vatankhah-Varnoosfaderani, J. Zhou, Q. Li and S. S. Sheiko, *Adv. Mater.*, 2015, **27**, 6899–6905.
18 Abbreviations shown in Fig. 1 and related references are as follows: DN = Double-network;[10] NC = Nanocomposite;[15] Agar or Alginate/PAAm = DNs of Agar or Alginate with polyacrylamide[11,13] PVA: Polyvinyl alcohol,[14] DMA/MAAc = *N*,*N*-dimethylacrylamide/methacrylic acid[17].
19 Y. Osada and J. Gong, *Prog. Polym. Sci.*, 1993, **18**, 187–226.
20 P. Egan, R. Sinko, P. R. LeDuc and S. Keten, *Nat. Commun.*, 2015, **6**, 7418.
21 A. Matsuda, J. Sato, H. Yasunaga and Y. Osada, *Macromolecules*, 1994, **27**, 7695–7698.
22 Y. Osada and A. Matsuda, *Nature*, 1995, **376**, 219.
23 Y. Tanaka, Y. Kagami, A. Matsuda and Y. Osada, *Macromolecules*, 1995, **28**, 2574–2576.
24 T. Miyazaki, K. Yamaoka, J. P. Gong and Y. Osada, *Macromol. Rapid Commun.*, 2002, **23**, 447.
25 T. Miyazaki, T. Kaneko, J. P. Gong and Y. Osada, *Macromolecules*, 2001, **34**, 6024.
26 M. Uchida, M. Kurosawa and Y. Osada, *Macromolecules*, 1995, **28**, 4583–4586.
27 X. K. Lin, L. Chen, Y. P. Zhao and Z. Z. Dong, *J. Mater. Sci.*, 2010, **45**, 2703–2707.
28 K. Inomata, T. Terahama, R. Sekoguchi, T. Ito, H. Sugimoto and E. Nakanishi, *Polymer*, 2012, **53**, 3281.
29 J. Hao and R. A. Weiss, *ACS Macro Lett.*, 2013, **2**, 89.
30 U. Nöchel, C. S. Reddy, N. K. Uttamchand, K. Kratz, M. Behl and A. Lendlein, *Eur. Polym. J.*, 2013, **49**, 2457–2466.
31 C. Bilici and O. Okay, *Macromolecules*, 2013, **46**, 3125–3131.
32 M. Balk, M. Behl, U. Nöchel and A. Lendlein, *Macromol. Mater. Eng.*, 2012, **297**, 1184–1192.
33 Y. Han, T. Bai, Y. Liu, X. Zhai and W. Liu, *Macromol. Rapid Commun.*, 2012, **33**, 225–231.
34 B. Kurt, U. Gulyuz, D. D. Demir and O. Okay, *Eur. Polym. J.*, 2016, **81**, 12–23.
35 C. Bilici, S. Ide and O. Okay, *Macromolecules*, 2017, **50**, 3647–3654.
36 C. Bilici, V. Can, U. Nöchel, M. Behl, A. Lendlein and O. Okay, *Macromolecules*, 2016, **49**, 7442–7449.
37 C. Bilici, D. Karaarslan, S. Ide and O. Okay, *Polymer*, 2018, **151**, 208–217.
38 A. Argun, U. Gulyuz and O. Okay, *Macromolecules*, 2018, **51**, 2437–2446.
39 V. I. Lozinsky and O. Okay, *Adv. Polym. Sci.*, 2014, **263**, 49–101.
40 V. P. Shibaev, B. S. Petrukhin, Y. A. Zubov, N. A. Plate and V. A. Kargin, *Vysokomol. Soedin., Ser. A*, 1968, **10**, 216.
41 N. A. Plate, V. P. Shibaev and B. S. Petrukhin, *Vysokomol. Soedin., Ser. B*, 1971, **13**, 757.
42 N. A. Plate and V. P. Shibvaev, *J. Polym. Sci., Part D: Macromol. Rev.*, 1974, **8**, 117.
43 C. E. Hoppe and R. J. J. Williams, *J. Colloid Interface Sci.*, 2018, **513**, 911–922.
44 Y. Geng, X. Y. Lin, P. Pan, G. Shan, Y. Bao, Y. Song, Z. L. Wu and Q. Zheng, *Polymer*, 2016, **100**, 60–68.
45 D. D. Wei, J. Yang, L. Zhu, F. Chen, Z. Q. Tang, G. Qin and Q. Chen, *ACS Appl. Mater. Interfaces*, 2018, **10**, 2946–2956.
46 D. C. Tuncaboylu, A. Argun, M. Sahin, M. Sari and O. Okay, *Polymer*, 2012, **53**, 5513–5522.
47 S. Abdurrahmanoglu, V. Can and O. Okay, *Polymer*, 2009, **50**, 5449–5455.
48 S. Abdurrahmanoglu, M. Cilingir and O. Okay, *Polymer*, 2011, **52**, 694–699.
49 W. J. Peer, Polymerization of hydrophobically modified polyacrylamide: effects of surfactants and comonomers, in *Polymers in Aqueous Media - Performance Through Association*, ed. J. E. Glass, Advances in Chemistry, American Chemical Society, 1989, vol. 223, pp. 381–397.
50 A. Hill, F. Candau and J. Selb, *Macromolecules*, 1993, **26**, 4521–4532.
51 F. Candau and J. Selb, *Adv. Colloid Interface Sci.*, 1999, **79**, 149–172.
52 D. C. Tuncaboylu, M. Sarı, W. Oppermann and O. Okay, *Macromolecules*, 2011, **44**, 4997–5005.
53 D. C. Tuncaboylu, M. Sahin, A. Argun, W. Oppermann and O. Okay, *Macromolecules*, 2012, **45**, 1991–2000.
54 E. Volpert, J. Selb and F. Candau, *Polymer*, 1998, **39**, 1025.
55 E. J. Regalado, J. Selb and F. Candau, *Macromolecules*, 1999, **32**, 8580.
56 B. Gao, H. Guo, J. Wang and Y. Zhang, *Macromolecules*, 2008, **41**, 2890.
57 V. Can, Z. Kochovski, V. Reiter, N. Severin, M. Siebenbürger, B. Kent, J. Just, J. P. Rabe, M. Ballauff and O. Okay, *Macromolecules*, 2016, **49**, 2281–2287.
58 O. Okay, *Adv. Polym. Sci.*, 2015, **268**, 101–142.
59 U. Gulyuz and O. Okay, *Macromolecules*, 2014, **47**, 6889–6899.
60 K.-H. Nitta and M. Takayanagi, *J. Macromol. Sci., Part B: Phys.*, 2003, **42**, 107–126.
61 K.-H. Nitta and M. Takayanagi, *J. Polym. Sci., Part B: Polym. Phys.*, 1999, **37**, 357–368.
62 J. P. Gong, *Soft Matter*, 2010, **6**, 2583–2590.
63 K. Sano, Y. Ishida and T. Aida, *Angew. Chem., Int. Ed.*, 2018, **57**, 2–14.
64 B. Yetiskin and O. Okay, *Polymer*, 2017, **112**, 61–70.
65 W. Wan, A. D. Bannerman, L. Yang and H. Mak, *Adv. Polym. Sci.*, 2014, **263**, 283–321.
66 T. Kaneko, D. Ogomi, R. Mitsugi, T. Serizawa and M. Akashi, *Chem. Mater.*, 2004, **16**, 5596–5601.
67 S. Choi and J. Kim, *J. Mater. Chem. B*, 2015, **3**, 1479–1483.
68 P. Lin, T. Zhang, X. Wang, B. Yu and F. Zhou, *Small*, 2016, **12**, 4386–4392.

69 S. H. Kim, S.-K. Im, S.-J. Oh, S. Jeong, E.-S. Yoon, C. J. Lee, N. Choi and E.-M. Hur, *Nat. Commun.*, 2017, **8**, 14346.
70 X. He, Y. Oishi, A. Takahara and K. Kajiyama, *Polym. J.*, 1996, **28**, 452–457.
71 W. Yang, H. Furukawa and J. P. Gong, *Adv. Mater.*, 2008, **20**, 4499–4503.
72 Z. L. Wu, T. Kurokawa, D. Sawada, J. Hu, H. Furukawa and J. P. Gong, *Macromolecules*, 2011, **44**, 3535–3541.
73 K. Cui, T. L. Sun, T. Kurokaw, T. Nakajimai, T. Nonoyama, L. Chenc and J. P. Gong, *Soft Matter*, 2016, **12**, 8833–8840.
74 H. Zhang, D. Han, Q. Yan, D. Fortin, H. Xia and Y. Zhao, *J. Mater. Chem. A*, 2014, **2**, 13373–13379.
75 J. Apostolakos, T. J. S. Durant, C. R. Dwyer, R. P. Russell, J. H. Weinreb, F. Alaee, K. Beitzel, M. B. McCarthy, M. P. Cote and A. D. Mazzocca, *Muscles Ligaments Tendons J.*, 2014, **4**, 333–342.
76 L. Rossetti, L. A. Kuntz, E. Kunold, J. Schock, K. W. Müller, H. Grabmayr, J. Stolberg-Stolberg, F. Pfeiffer, S. A. Sieber, R. Burgkart and A. R. Bausch, *Nat. Mater.*, 2017, **16**, 664–670.
77 N. L. Nerurkar, D. M. Elliott and R. L. Mauck, *J. Biomech.*, 2010, **43**, 1017–1030.
78 B. R. Whatley and X. Wen, *Mater. Sci. Eng., C*, 2012, **32**, 61–77.
79 J. C. Iatridis, S. B. Nicoll, A. J. Michalek, B. A. Walter and M. S. Gupta, *Spine J.*, 2013, **13**, 243–264.
80 T. Sauter, M. Heuchel, K. Kratz and A. Lendlein, *Polym. Rev.*, 2013, **53**, 6–40.
81 I. Bellin, S. Kelch, R. Langer and A. Lendlein, *Proc. Natl. Acad. Sci. U. S. A.*, 2006, **103**, 18043–18047.
82 H. J. Jin and D. L. Kaplan, *Nature*, 2003, **424**, 1057.

